Asymmetry of Nonlinear Transport and Electron Interactions in Quantum Dots

D. M. Zumbühl and C. M. Marcus
Department of Physics, Harvard University, Cambridge, Massachusetts 02138, USA

M. P. Hanson and A. C. Gossard
Materials Department, University of California, Santa Barbara, California 93106, USA

(Received 31 August 2005; published 25 May 2006)

The symmetry properties of transport beyond the linear regime in chaotic quantum dots are investigated experimentally. A component of differential conductance that is antisymmetric in both applied source-drain bias V and magnetic field B, absent in linear transport, is found to exhibit mesoscopic fluctuations around a zero average. Typical values of this component allow a measurement of the electron interaction strength.

DOI: 10.1103/PhysRevLett.96.206802 PACS numbers: 73.23.Hk, 73.20.Fz, 73.50.Gr

Quantum transport in disordered mesoscopic conductors and chaotic quantum dots has been widely studied in the regime of linear response, and is well understood in terms of universal statistical theories [1], even in the presence of significant electron interaction [2,3]. A central principle of linear mesoscopic transport concerns the symmetry of magnetoconductance: as a consequence of time-reversal symmetry and microscopic reversibility close to equilibrium, the differential conductance $g = dI/dV$ of a two-terminal sample is symmetric in magnetic field B: $g(B) = g(-B)$ [4–6], with generalized reciprocity (Landauer-Büttiker) relations for multiterminal coherent conductors [6] allowing asymmetry in B of linear response functions, as discussed, e.g., in Ref. [7]. Beyond linear response, i.e., when the current I is no longer proportional to the source-drain voltage V, these symmetry relations break down. Unless disallowed by some special symmetry, differential conductance beyond linear response can generally contain a component (here denoted $\tilde{g}$) that is proportional to both B and V:

$$\tilde{g} = \alpha V B. \tag{1}$$

For instance, contributions to g of the form in Eq. (1) are permitted in non-centro-symmetric materials [8], chiral conductors [9], including carbon nanotubes [10], or conductors with crossed electric and magnetic fields [11].

In the absence of electron interaction, including indirect interaction such as inelastic phonon scattering, the coefficient α in Eq. (1) vanishes, since conduction at each energy within the finite bias window independently obeys the symmetry of linear response and different energies do not mix [12,13]. Moreover, as discussed recently in Refs. [14,15], α is proportional to the electron interaction strength, suggesting that terms of the form of Eq. (1) can be used to measure the interaction strength. We emphasize that in coherent transport through quantum dots, $\tilde{g}$ has mesoscopic fluctuations similar to fluctuations of linear conductance, and is suppressed by dephasing and thermal averaging, as pointed out in Refs. [14,15].

This Letter presents a detailed study of the symmetry of nonlinear conductance in an open chaotic GaAs quantum dot, using gate-controlled shape distortion to gather ensemble statistics. We focus on the component of g that is antisymmetric in B, denoted g_{B-} (see Fig. 1) and find that g_{B-} is largely antisymmetric in V. For small $V \lesssim \Delta/e$ and $B \lesssim \phi_0/A$, where Δ is the average quantum level spacing in the dot and $\phi_0 = h/e$ is the flux quantum, g_{B-} is of the

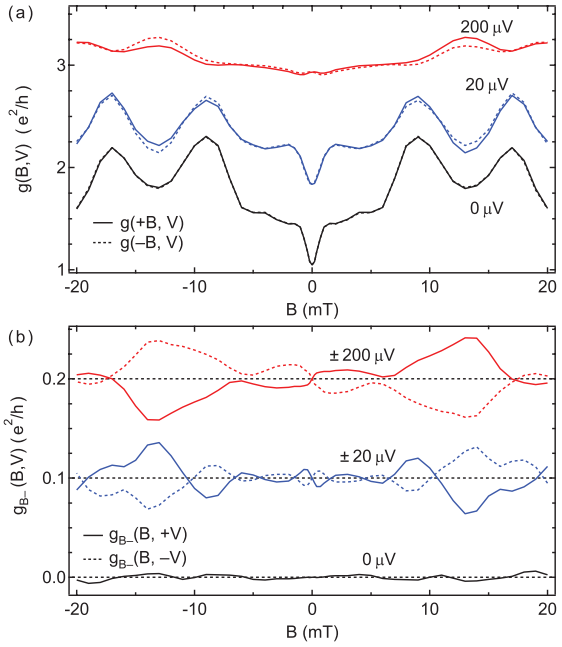

FIG. 1 (color). (a) Differential conductance g for $N = 2$ as a function of magnetic field B (solid curves) and $-B$ (dashed curves) at source-drain bias V as indicated, at base electron temperature $T_{el} = 45$ mK. The blue (red) curves are offset by $+0.5(+1)e^2/h$, respectively. (b) Antisymmetric in B conductance g_{B-} of the traces shown in (a), as a function of B at V (solid curves) and $-V$ (dashed curves) as indicated. The blue (red) curves are offset by $+0.1(+0.2)e^2/h$, respectively. Black curves demonstrate $g(B, V = 0) = g(-B, V = 0)$ and blue or red curves indicate g_{B-} is largely antisymmetric in V.

form Eq. (1). Further g_{B-} shows mesoscopic fluctuations as a function of B, V, and shape-gate voltage V_G, as anticipated theoretically [14,15]. The average coefficient α measured over an ensemble of dot shapes vanishes and the standard deviation of α, denoted $\delta\alpha$, is used to characterize the interaction strength. The theory [14,15] is compared with the experimental $\delta\alpha$ for $N = 1, 2, 4$ modes in the quantum-point contacts, giving reasonable agreement only for $N = 4$. However, present theories [14,15] assume that electrons do not thermalize within the dot and neglect effects of decoherence, temperature, and imperfect mode transmission.

Measurements were carried out using a quantum dot of area $A \sim 1\ \mu\text{m}^2$ formed by Ti/Au depletion gates [see Fig. 2(d)] on the surface of a $GaAs/Al_{0.3}Ga_{0.7}As$ heterostructure 105 nm above the 2D electron gas. A bulk electron density $n \sim 2 \times 10^{11}\ \text{cm}^{-2}$ and mobility $\mu \sim 2 \times 10^5\ \text{cm}^2/\text{V s}$, giving a mean free path $l \sim 1.5\ \mu\text{m}$, indicates ballistic transport within the dot. This device contains $N_{\text{dot}} \sim 2000$ electrons and has an average level spacing $\Delta = 2\pi\hbar^2/m^*A \sim 7\ \mu\text{eV}$, where $m^* = 0.067m_e$ is the effective electron mass. The dot was designed to lack spatial symmetry [17] and is found to show universal statistics characteristic of chaotic classical dynamics in the linear conduction of the device [1–3]. The gate marked "shape," with voltage V_G applied, was used to modify the dot boundary, providing a means of generating ensemble statistics [18]. Gates $w1$ and $w2$ were trimmed to keep both point contacts on the same quantized conductance plateau as the shape-distorting gate V_G was swept to gather ensemble statistics. Gates $p1$ and $p2$ were strongly depleted, isolating the adjacent smaller dot, which was used only to measure the electron temperature ($T_{\text{el}} = 45 \pm 5$ mK at base) using Coulomb blockade peak width [19].

To measure g, simultaneous lock-in measurements of both differential current and voltage across the dot were made using a four-wire setup at 94.7 Hz with typical ac excitation of 2 μV, in the presence of a dc source-drain voltage V. All voltages were applied symmetrically across the dot [Fig. 2(a)] to reduce any circuit induced bias voltage asymmetry to less than 5% of the applied V throughout the experiment, making self-gating effects [17] negligible. $g(B, V, V_G)$ was measured as a function of V (innermost loop) and B (2nd loop, with higher point density around zero field). Each of these two-parameter sweeps was repeated 20 times to reduce noise (3rd loop), for each of 16 statistically independent shape gate voltages V_G (4th loop). Each multiparameter sweep, which took about 30 h to complete, was measured at $N = 1, 2, 4$ modes in each lead (outermost loop).

As expected for a two-terminal device [4–6], the linear conductance $g(B, V = 0)$ was found to be symmetric in B within measurement resolution, as seen in the black trace in Fig. 1(a). At finite bias, however, the $\pm B$ symmetry is broken, as seen in the blue and red traces in Fig. 1(a). Decomposing g into components that are symmetric (g_{B+}) and antisymmetric (g_{B-}) in field, $g_{B\pm}(B, V) = [g(B, V) \pm g(-B, V)]/2$, we find $g_{B-}(B, V = 0)$ comparable to the measurement noise of $3 \times 10^{-3}e^2/h$ [black trace in Fig. 1(b)], while at $V = \pm 20\ \mu\text{eV}$ and $\pm 200\ \mu\text{eV}$, g_{B-} is readily seen in the data and is found to be largely antisymmetric in V [blue and red traces in Fig. 1(b)]. The typical amplitude of fluctuations of g_{B-} is $\sim 0.025e^2/h$, much smaller than the amplitude of fluctuations of g, which is $\sim 0.5e^2/h$.

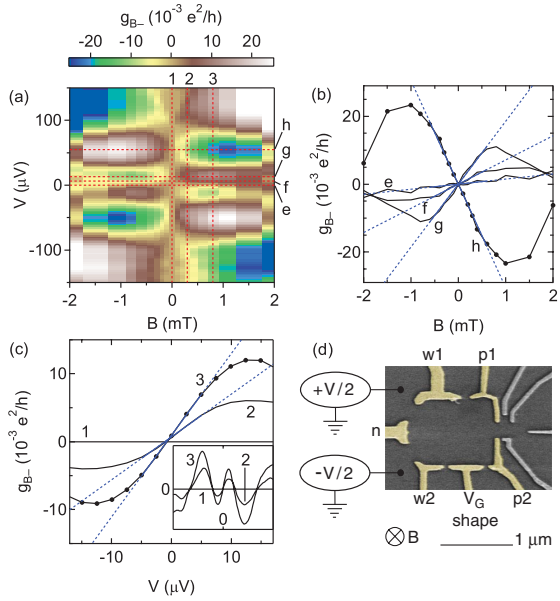

FIG. 2 (color). (a) Antisymmetric component g_{B-} (color scale) as a function of B and V at $N = 2$. Dashed lines indicate cuts shown in (b) and (c). (b) g_{B-} as a function of B at $V = 0, 7.5, 15, 55\ \mu\text{V}$. (c) g_{B-} as a function of V at $B = 0, 0.3, 0.8$ mT. Linear fits to curves in (b) and affine ($y = ax + b$) fits to curves in (c) are shown in dashed blue lines, with solid blue lines indicating the fitting range. For extraction of α, the constant term in fits (c) is held at zero ($b = 0$), equivalent to fitting to g_{B-V-} fully antisymmetrized in both B and V. Inset to (c) shows the same cuts as in (c) with the V axis extended to $\pm 125\ \mu\text{V}$ and the g_{B-} axis extended to $\pm 25 \times 10^{-3}e^2/h$. (d) Electron micrograph of a device with the same gate design as the one measured. Only the yellow gates are used in this experiment. V is applied symmetrically.

The antisymmetry of $g_{B-}(B, V)$ in source-drain voltage V is also seen in Fig. 2(a), which shows $g_{B-}(B, V)$ for $N = 2$ as a 2D color plot for a different shape sample than the one shown in Fig. 1. Note that $g_{B-}(B, V)$ changes sign repeatedly as a function of both B and V. Similar characteristics are seen for all dot shapes and values of N, though for some shape samples the antisymmetry in V is more pronounced than in others.

For small fields, $B \lesssim \phi_0/A$, $g_{B-}(B)$ is proportional to B and is fully developed for $V \gtrsim \Delta/e \sim 7\ \mu\text{eV}$, as seen in Fig. 2(b). At larger fields, $B \gtrsim \phi_0/A$, $g_{B-}(B)$ shows mesoscopic fluctuations as a function of B, including sign changes. The field scale where this crossover occurs is consistent with the field scale of weak localization [see Fig. 3(a)] and conductance fluctuations in this device (not

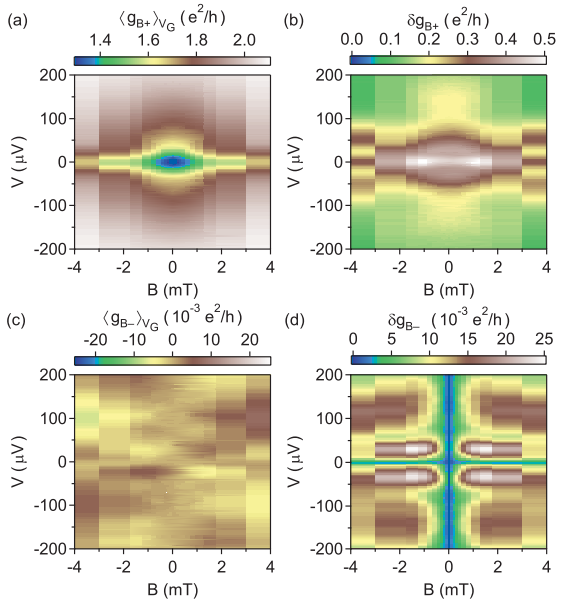

FIG. 3 (color). Average conductance component $\langle g_{B+}\rangle_{V_G}$ (a) and $\langle g_{B-}\rangle_{V_G}$ (c) and standard deviation δg_{B+} (b) and δg_{B-} (d) (color scale) obtained from 16 independent shape samples at $N = 2$ modes as a function of B and V. $\langle g_{B-}\rangle$ is zero within statistical uncertainty; standard deviations are used to characterize the antisymmetries. $\langle g_{B+}\rangle$ shows a strong dip at $(B, V) = 0$ due to ballistic weak localization.

shown). This field scale is somewhat smaller than $\phi_0/A \sim 4$ mT, similar to previous experiments [20,21], because the relevant area is $\sim\sqrt[4]{N_{\rm dot}}$, the area of typical trajectories before escape [22]. For $V \lesssim \Delta/e$, $g_{B-}(V)$ is also found to be proportional to V and becomes fully developed for $B \gtrsim 1$ mT, as seen in Fig. 2(c). For $V \gtrsim \Delta/e$, $g_{B-}(V)$ starts to deviate from the linear dependence on V and shows mesoscopic fluctuations as a function of V, also including sign changes. The characteristic scales $V \sim \Delta/e$ and $B \sim \phi_0/A$ for mesoscopic fluctuations of $g_{B-}(B, V)$ provide assurance that this component arises from coherent transport within the dot.

The average symmetric component of conductance, $\langle g_{B+}\rangle_{V_G}$, which is maximal around $V = 0$, has a pronounced minimum around $B = 0$ due to ballistic weak localization [23], as seen in Fig. 3(a). From the magnitude of the weak localization feature in $\langle g(B, V = 0)\rangle_{V_G}$, we extract a base-temperature phase coherence time $\tau_\varphi \sim 2$ ns, consistent with previous experiments [23]. As seen in Fig. 3(a), finite V reduces the dip $\langle g(B, V = 0)\rangle_{V_G}$ around $B = 0$, presumably the result of dephasing caused by heating and nonequilibrium effects [24,25]. Figure 3(b) shows that the standard deviation of the symmetric component δg_{B+} is peaked around $B = 0$, a well-known effect associated with breaking of time-reversal symmetry [1–3,18]. Similar to the weak localization correction, δg_{B+} is also reduced at finite bias. In this case, the reduction is due both to dephasing and an explicit dependence on temperature and energy averaging.

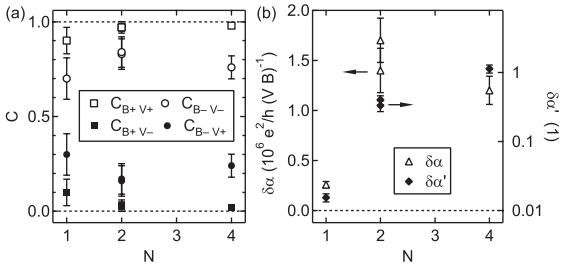

FIG. 4. (a) Normalized symmetry parameter C as a function of the number of modes N for all B and V symmetries as indicated, giving a statistical characterization of the nonlinear field symmetry properties of conductance over all V, B and shape samples measured. (b) Standard deviation $\delta\alpha$ (open triangles) and dimensionless standard deviation $\delta\alpha'$ (solid diamonds) of the interaction parameter (see text) as a function of N.

Figure 3(c) shows the shape-averaged antisymmetric component of conductance $\langle g_{B-}\rangle_{V_G}$, which is zero within statistical uncertainty (based on 16 shape samples), indicating that fluctuations of g_{B-} cancel each other upon averaging, as predicted theoretically [14,15]. As seen in Fig. 3(d), the standard deviation δg_{B-} becomes fully developed on a V scale of order of the dot level spacing, with a maximum at moderate $|V|$, and then decreases for larger $|V|$, presumably due to heating or decoherence effects. By definition, δg_{B-} is zero for $B = 0$ and, as expected for a g_{B-} largely antisymmetric in V, δg_{B-} is comparable to the statistical error along the $V = 0$ line.

To characterize symmetry in terms of statistical quantities, we define normalized symmetry parameters $C_{B\pm V\pm} = \delta^2 g_{B\pm V\pm}/\delta^2 g_{B\pm}$, where $\delta^2 g_{B\pm V\pm}$ is the variance of the component of g with a particular symmetry with respect to B and V [26]. Here, ensemble averaging is performed over the entire (B, V, V_G) parameter space, resulting in approximately $5 \times 4 \times 16$ independent samples. We note that C ranges from zero to one, $C_{B+V+} + C_{B+V-} = 1$ and $C_{B-V+} + C_{B-V-} = 1$. As seen in Fig. 4, $C_{B+V+} \sim 1$ (open squares) and $C_{B+V-} \sim 0$ (solid squares) within the statistical uncertainty, showing that g_{B+} is symmetric in V for all measured conductance samples and mode numbers N. $C_{B-V-} \sim 0.75$ (open circles) and $C_{B-V+} \sim 0.25$ (solid circles) without a strong N dependence, indicating that a significant part of g_{B-} is antisymmetric in V, though the antisymmetry is not perfect. The physics that sets the relative weighting of $C_{B-V\pm}$ is not understood as far as we know.

The interaction coefficient α was extracted for each shape by fitting a function linear in both B and V (without constant term) to $g_{B-}(B, V)$ for small $V < \Delta/e$ and $B < \phi_0/A$, similar to the fits shown in Figs. 2(b) and 2(c). The resulting α has mesoscopic fluctuations and changes sign frequently, consistent with $\langle\alpha\rangle_{V_G} = 0$ within statistical uncertainty. The standard deviation $\delta\alpha$, used to characterize the strength of electron interaction, is shown in Fig. 4(b) (open triangles) as a function of the mode number N.

For a comparison of the interaction parameter α to theory, we note that Ref. [15] predicts $\delta\alpha$ for $kT \ll N\Delta$, $V \ll \Delta/e$ and $B \ll \phi_0/A$:

$$\delta\alpha = \delta\alpha' \frac{1}{2N^2} \frac{e}{\Delta} \frac{A}{\phi_0} \frac{e^2}{h}, \quad (2)$$

where $\delta\alpha'$ is a dimensionless parameter characterizing the electron interaction strength. The form in Eq. (2) is obtained from Eq. 4 in Ref. [15] by taking $\nu = m^*/(2\pi\hbar^2)$ and replacing the escape broadening $\Gamma = \hbar D/A$ for a diffusive sample (diffusion constant D) by the escape broadening, $\Gamma = N\Delta/\pi$, for a ballistic-chaotic dot with N channel leads. Reference [14] derives a similar expression for $\delta\alpha$ that is directly applicable to ballistic-chaotic dots and also allows for different numbers of modes in the two leads [27]. To facilitate a comparison of experiment and theory, we plot the dimensionless quantity $\delta\alpha'$ in Fig. 4(b), noting a pronounced dependence of $\delta\alpha'$ on N. As defined in Eq. (2), $\delta\alpha'$ is not expected to depend on N, according to Refs. [14,15]. We speculate that for $N < 4$, the escape time from the dot is sufficiently long so that electrons have time to restore effective equilibrium in the dot (as in linear transport), though at a higher effective temperature. Because a finite asymmetry $\delta\alpha'$ requires departure from equilibrium, $\delta\alpha'$ is reduced at $N = 1, 2$ compared to $N = 4$. This hypothesis is supported by direct measurements of electron distribution functions in the same device [16], which show that for $N = 1$ the distribution of electron energies in the dot is thermal, with an elevated effective temperature that depends on V. For $N = 4$, on the other hand, with a shorter electron dwell time in the dot, nonthermal distributions are found [16]. For the case $N = 4$, the measured $\delta\alpha' = 1.1 \pm 0.2$ is of the same order as the theoretical estimate $\delta\alpha' = \pi/2$ [27], which assumes perfect screening of electrons. For $N = 1, 2$ the discrepancy between the measured and predicted $\delta\alpha'$ is considerably greater (a factor of 5 for $N = 2$ and a factor of 100 for $N = 1$), as seen in Fig. 4(b). Other factors that may contribute to the observed N dependence of $\delta\alpha'$ include imperfectly transmitting modes or mode mixing as well as finite temperature and/or decoherence effects, all of which are not currently accounted for theoretically. It remains for future work to settle this issue conclusively.

In conclusion, we have investigated the magnetic field asymmetry of conductance beyond the linear regime in gate-defined quantum dots. The conductance component g_{B-}, which is defined to be antisymmetric in B, was found to be also predominantly antisymmetric in V and is of the form of Eq. (1) for $V \ll \Delta/e$ and $B \ll \phi_0/A$. The interaction coefficient α, extracted from linear fits to g_{B-}, has mesoscopic fluctuations with zero average. Comparison to recent theory [14,15] is most appropriate for the data with four modes per lead, where electrons remain out of equilibrium during the short dwell time. In this case, consistency with theory [14] relating α to the interaction strength appears reasonable, suggesting good electron screening.

We thank B. Spivak for suggesting this problem to us and M. Büttiker and D. Sanchez for numerous contributions. This work was supported in part by DARPA under QuIST, ARDA/ARO Quantum Computing Program, and Harvard NSEC. Work at UCSB was supported by QUEST, an NSF Science and Technology Center.

Note added.—During completion of this work, related experimental work on carbon nanotubes appeared [28].

[1] C. W. J. Beenakker, Rev. Mod. Phys. **69**, 731 (1997).
[2] I. L. Aleiner, P. W. Brouwer, and L. I. Glazman, Phys. Rep. **358**, 309 (2002).
[3] Y. Alhassid, Rev. Mod. Phys. **72**, 895 (2000).
[4] L. Onsager, Phys. Rev. **38**, 2265 (1931).
[5] H. G. B. Casimir, Rev. Mod. Phys. **17**, 343 (1945).
[6] M. Büttiker, Phys. Rev. Lett. **57**, 1761 (1986).
[7] H. van Houten *et al.*, Phys. Rev. B **39**, 8556 (1989).
[8] B. I. Sturman and V. M. Fridkin, *The Photovoltaic and Photorefractive Effects in Non-Centrosymmetric Materials* (Gordon and Breach, New York, 1992).
[9] G. L. J. A. Rikken, J. Fölling, and P. Wyder, Phys. Rev. Lett. **87**, 236602 (2001).
[10] E. L. Ivchenko and B. Spivak, Phys. Rev. B **66**, 155404 (2002).
[11] G. L. J. A. Rikken and P. Wyder, Phys. Rev. Lett. **94**, 016601 (2005).
[12] A. Larkin and D. Khmel'nitskii, Sov. Phys. JETP **64**, 1075 (1986); Phys. Scr. **T14**, 4 (1986).
[13] V. Fal'ko and D. Khmel'nitskii, Sov. Phys. JETP **68**, 186 (1989).
[14] D. Sanchez and M. Büttiker, Phys. Rev. Lett. **93**, 106802 (2004); Int. J. Quantum Chem. **105**, 906 (2005).
[15] B. Spivak and A. Zyuzin, Phys. Rev. Lett. **93**, 226801 (2004).
[16] D. M. Zumbühl *et al.* (to be published).
[17] A. Löfgren *et al.*, Phys. Rev. Lett. **92**, 046803 (2004).
[18] I. H. Chan *et al.*, Phys. Rev. Lett. **74**, 3876 (1995).
[19] L. P. Kouwenhoven *et al.*, in *Mesoscopic Electron Transport*, edited by L. L. Sohn, L. P. Kouwenhoven, and G. Schön (Kluwer, Dordrecht, 1997).
[20] C. M. Marcus *et al.*, Phys. Rev. Lett. **69**, 506 (1992).
[21] D. M. Zumbühl *et al.*, Phys. Rev. B **72**, 081305 (2005).
[22] C. M. Marcus *et al.*, Chaos Solitons Fractals **8**, 1261 (1997).
[23] A. G. Huibers *et al.*, Phys. Rev. Lett. **83**, 5090 (1999).
[24] M. Switkes *et al.*, Appl. Phys. Lett. **72**, 471 (1998).
[25] H. Linke *et al.*, Phys. Rev. B **56**, 14 937 (1997).
[26] $g_{B+}V_{\pm} = \frac{1}{2}[g_{B+}(B, V) \pm g_{B+}(B, -V)]$ and $g_{B-}V_{\pm} = \frac{1}{2}[g_{B-}(B, V) \pm g_{B-}(B, -V)]$.
[27] Up to the magnetic field scale A/ϕ_0, Eq. (2) follows from the square root of Eq. 10 in Ref. [14] by setting $N_1 = N_2 = N$. A factor of 2 needs to be included for the definition of Φ via current I rather than $g = dI/dV$, giving $\delta\alpha' = \pi/2(C_\mu/C)$ (for spin degenerate electrons).
[28] J. Wei *et al.*, Phys. Rev. Lett. **95**, 256601 (2005).